

Figure S1 Multiple sequence alignment of talin F1 domain loops, with snapshots from molecular dynamics simulations to highlight the proposed functions of the different parts of the F1 loop. A) The L152 residue, and occasionally L151, entered the hydrophobic core of the membrane. B) The D154 interfered with the salt bridge between α IIb R995 and β 3 D723. Additional salt bridges between E155 and R997 were occasionally observed. C) Integrin clustering tests of talin t1-435 to evaluate the contribution of L151, L152 and R153 for integrin clustering. Clustering defects are not visible in individual R153A-mutants 151-154LLAD, or in the LLRD/AARA mutant, proposing redundant functions of residues involved in membrane binding and charge interference. One-way ANOVA ($F(3,8)=6.909$, $p=0.013$) and Tukey's multiple comparison test showed that talin t1-435(D154A,E154A) clustered integrins less efficiently ($p < 0.05$) than the other talin forms analyzed, $n=3$. D) Effects of phosphomimicking and phosphoblocking mutations of T144 and T150 on integrin clustering. Clustering indices and mean. Statistical significance was assessed with one-way ANOVA ($F(5,20)=25.48$, $p<0.0001$) and Tukey's multiple comparison test. For t1-435 ±Kind1 and t1-435(T144E,T150E) ±Kind1: $n=5$ experiments, and for t1-435(T144A,T150A): $n=3$. E) The molecular dynamics simulation snapshots A-B and I-J mapped onto the talin-integrin-membrane model. F) Multiple sequence alignment of talin sequences from *Homo sapiens* Q9Y490, *Gallus gallus* NP_989854.1, *Brachydanio rerio* NP_001009560.1, *Branchiostoma belcheri* XP_019621066.1, *Strongylocentrotus purpuratus* XP_011673604.1, *Lottia gigantea* ESO89699.1, *Capitella teleta* ELU05070.1, *Amphimedon queenslandica* XP_011410411.1, *Drosophila melanogaster* Q9VSL8, *Anopheles gambiae* str. PEST AGAP007474-PA, *Trichoplax adhaerens* XP_002108146.1, and *Dictyostelium discoideum* sequences P0CE94 and Q54K81. The alignment was generated with the MUSCLE algorithm implemented in MEGA7 (Edgar, 2004; Kumar et al., 2016). G) Average formal charges of the alignment positions. H) Conservation of the alignment positions calculated using the Jensen-Shannon divergence scoring (Capra and Singh, 2007) (<http://compbio.cs.princeton.edu/conservation/score.html>). PIP2 lipid contacts formed both upstream (I) and downstream (J) of the integrin interaction site in the loop. Occupancy was calculated as the average number of PIP2 lipids within a distance of 4 Å from the amino acid residue. K) Root mean square fluctuations (RMSF) of the F1 loop residues in molecular dynamics simulations. Data from simulations with talin-integrin complex at a DOPC and PIP2 containing membrane (DOPC+PIP2) or talin head alone in solution (no lipids). RMSF was calculated using the RMSD Visualizer Tool in VMD, with a frame frequency of 1/100 ps. Please note that Threonine phosphorylations (P) in F, were identified in the case of P^a by Stuart et al., in the case of P^b by Ratnikov et al., and in the case of P^c by Dephoure et al. (Stuart et al., 2015; Ratnikov et al., 2005; Dephoure et al., 2008). Please also note the regions c-terminal of the integrin binding site, involved in interactions with the F3 (yellow) and F2 (olive) subdomains and shown in Fig. 5B and Fig. 5C, respectively.

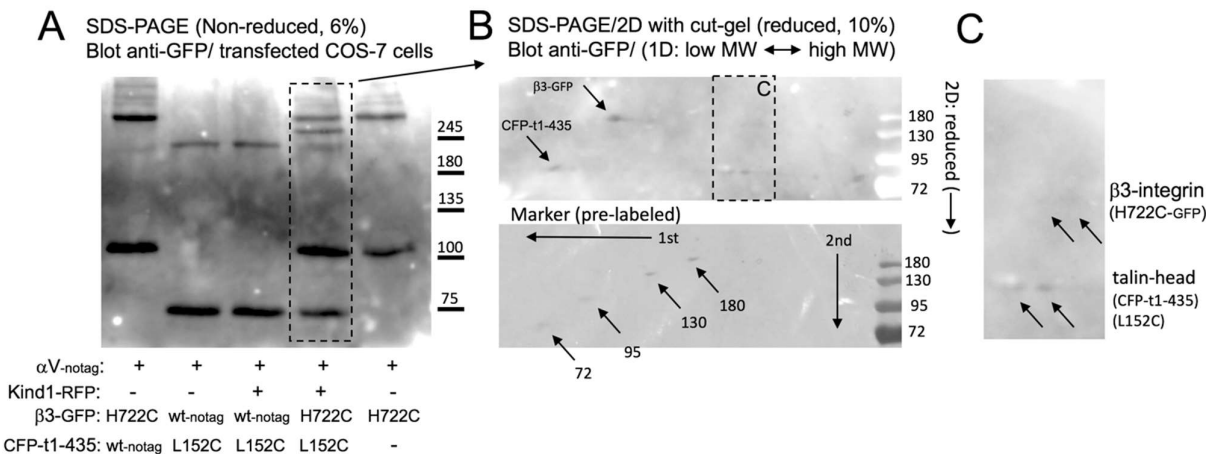


Figure S2 Cysteine cross-linking analysis of individual talin head and integrin mutants and 2D SDS-PAGE (non-reduced/reduced). A) 6% SDS-PAGE and western blot revealed with mAb anti-GFP/anti-mouse HRP of copper/phenanthroline oxidized lysates of COS7 cells transfected with the indicated constructs. Blot is slightly overexposed to detect high molecular weight, multimeric GFP, or CFP-containing protein bands. B) Second dimension of a 2D SDS-PAGE (non-reduced 6%/reduced 10%) and subsequent western blot of a cut vertical gel lane, containing the identical sample as boxed with dashed lines in A. Adjacent marker proteins separated in the first dimension were also loaded together with the cut-out gel, providing a 2D-migration space to identify the revealed GFP or CFP tagged proteins (indicated with arrows). Please note the slower migration of the β3-GFP-integrin band in the second (reduced) dimension due to multiple intramolecular cys-bridges. Please note also that different pre-stained marker proteins were used in the two blots/experiments. C). Blow up of the boxed region in B. Arrows are pointing to anti-GFP (CFP) reactive protein bands, migrating at the level of the CFP-talin head (CFP-t1-435(L1542C)) and β3-GFP-integrin (H722C), revealing the middle of the three upper bands in A, as containing talin head and β3-integrin (see also figure 4B).

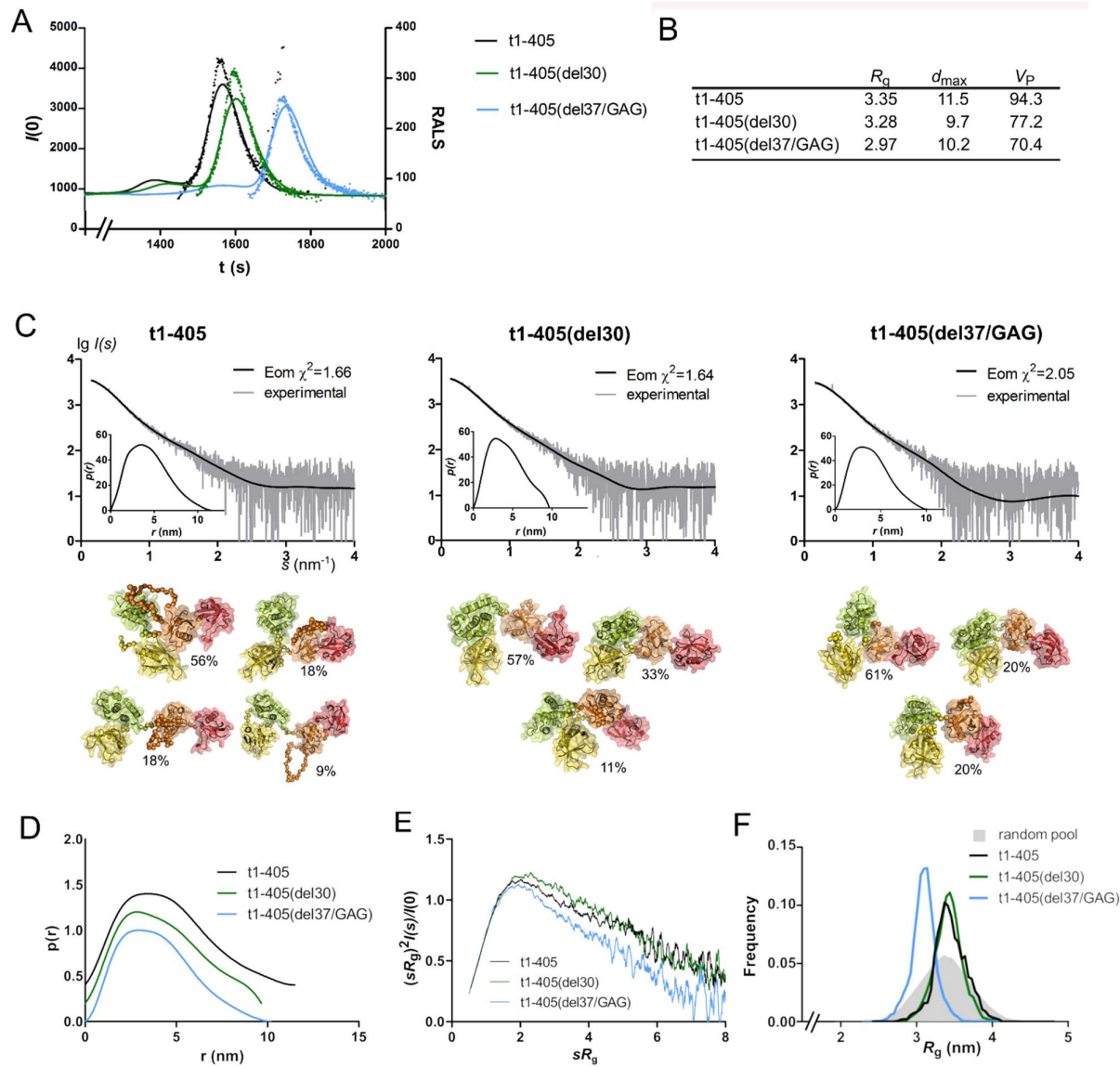


Figure S3 Protein shape determination by SAXS. A) Right-angle light scattering (RALS; solid line) and SAXS forward scattering ($I(0)$; dots) curves fitted with GNU Octave 4.0.0 (Eaton et al., 2015). Data from the monomeric peak were used in SAXS analysis. B) Radius of gyration (R_g), particle maximum dimension (d_{\max}), and Porod volume (V_p). C) The SAXS data and the fit of the ensemble model (Eom). Particle distance distribution function is shown as an insert. Models representative of the conformational ensemble in solution, modeled with Eom using individual subdomain X-ray structures, are shown in a cartoon and surface representation below the scattering data. The F1 loop and linkers were modeled *ab initio*, and are shown as spheres. D) Normalized particle distance distribution functions of the three talin head forms. E) Dimensionless Kratky plots ($(sR_g)^2 I(s)/I(0)$) as a function of sR_g . F) Radius of gyration distributions in Eom-generated ensemble models. The R_g distributions of the random pools are shown in gray.

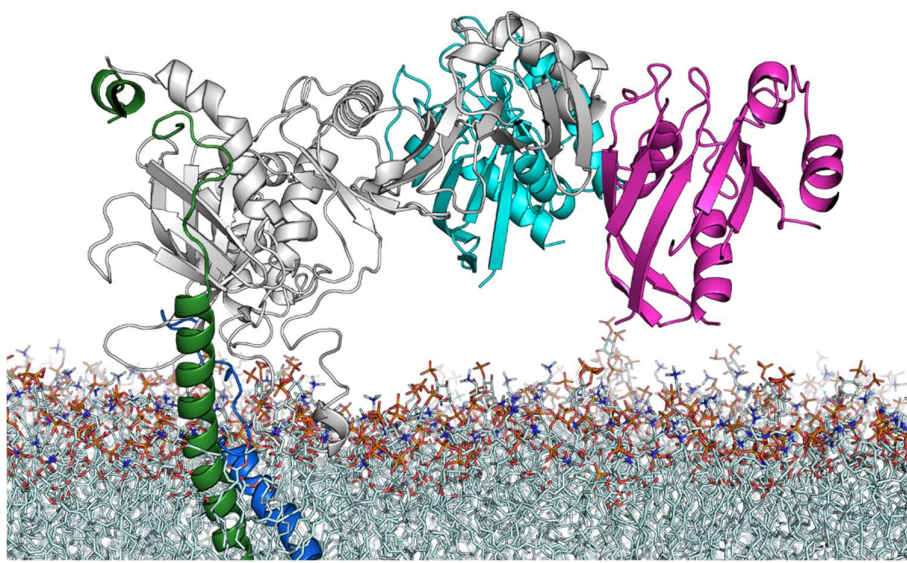


Figure S4 Model of Rap1b binding to a FERM-folded talin. Rap1b in complex with talin F0 (NMR structure, PDB: 6BA6 (Zhu et al., 2017)) was aligned with the F0 (Rap1b in magenta) and F1 (Rap1b in cyan) subdomains of our talin FERM model in a snapshot from MD simulation. Light gray: talin, blue: α -integrin, green: β -integrin.

Table S1 Mass spectrometry of human talin head constructs. Each construct included an N-terminal purification tag MGGSHHHHHGMASMTGGQQMGRDLYDDDKDRWIRPRA. Mass error is given for forms without initiator methionine.

Construct	Theoretical mass (Da)	Theoretical mass (Da) without Met	Experimental mass (Da)	Mass error (Da)
t1-405	51406.30	51275.20	51275.20	+0.00
t1-405(del30)	47798.35	47666.52	47666.31	+0.21
t1-405(del37/GAG)	47089.24	46958.02	46958.20	+0.18
t1-405(T144E,T150E)	51462.34	51331.30	51331.71	+0.41
t1-405(151-154AAAA)	51193.20	51061.16	51061.27	+0.11
t206-405	27523.07	27391.03	27391.10	+0.07

Table S2 Characterization of talin forms by size-exclusion chromatography (SEC) equipped with in-line static (SLS) and dynamic light scattering (DLS), and analysis of melting temperature (T_m) in differential scanning calorimetry. Theoretical molecular weight ($MW_{theor.}$) and molecular weight determined by SEC-SLS (MW_{SLS}) are given in kDa. Retention volume (V_r) is given in ml. Hydrodynamic radius $R(h)$ is given in nm. Melting temperature T_m and the difference from T_m (t1-405) (ΔT_m) are given in °C. Binding of wild-type (WT- $\beta 3$) and high-affinity (VE- $\beta 3$)(Pinon et al., 2014) $\beta 3$ -integrin was analyzed using the ForteBio Octet RED384 optical biosensor. The approximated Gibbs free energy of binding (ΔG_{app}) and the difference in ΔG_{app} compared to t1-405 ($\Delta \Delta G_{app}$), are shown in kJ mol⁻¹. Please note that the GST protein used as a carrier for the integrin peptide in this experiment is dimeric.

talin	$MW_{theor.}$	HPLC				DSC		Integrin binding			
		V_r	MW_{SLS}	$R(h)$ in DLS		T_m	ΔT_m	WT- $\beta 3$	VE- $\beta 3$	ΔG_{app}	$\Delta \Delta G_{app}$
t1-405	51.4	1.80	66.9	4.62 ± 0.35		54.2 ± 0.1	0	-27.1	0.0	-37.1	0.0
t1-405(del30)	47.8	1.90	65.3	4.48 ± 0.30		55.4 ± 0.1	+1.1	-27.9	-0.7	-38.1	-1.0
t1-405(del37/GAG)	47.1	1.88	64.9	4.48 ± 0.37		57.0 ± 0.3	+2.8	-29.1	-1.9	-37.3	-0.3
t1-405(T144E,T150E)	51.5	1.80	68.6	4.55 ± 0.28		54.2 ± 0.5	0	-24.1	+3.0	-34.6	+2.5
t1-405(151-154AAAA)	51.2	1.80	67.7	4.59 ± 0.35		54.2 ± 0.2	-0.1	-26.3	+0.9	-35.1	+2.0
t206-405	27.7	2.13	33.2	3.30 ± 0.30		56.2 ± 0.4	+2.0	-40.3	-13.1	-37.9	-0.8

Table S3 Molecular dynamics simulation setup. All simulations were carried out in the OPLS-AA force field.

Simulation	Talin	Integrin	DOPC	PIP2	Waters	K ⁺	Cl ⁻	#atoms	time
PIP-A	+	+	844	96	127343	356	356	522623	1 μs
PIP-B	+	+	844	96	127343	356	356	522623	1 μs
no-PIP-A	+	+	950	-	114249	318	324	483313	500 ns
no-PIP-B ^a	+	+	950	-	136471	382	388	550107	1 μs
t1-405	+	-	-	-	60670	171	180	189001	100 ns
control-A	-	+	420	50	56182	358	155	236603	750 ns
control-B	-	+	420	50	56182	358	155	236603	750 ns

^a Starting conformation of the protein adopted from PIP-A at t=20 ns.

Table S4 DSS crosslinking mass spectrometry of F1 loop containing t1-405 talin head construct. List of observed contacts. Location of the residues within the talin head is given in parentheses. F1L: F1 loop.

Involving F1 loop residues		Intra-subdomain or intra-F1 loop		Inter-subdomain	
Residue 1	Residue 2	Residue 1	Residue 2	Residue 1	Residue 2
K149 (F1L)	K268 (F2)	K138 (F1L)	K160 (F1L)	K84 (F0-F1 linker)	K106 (F1)
K149 (F1L)	K320 (F3)	K324 (F3)	K343 (F3)	K272 (F2)	K343 (F3)
K98 (F1)	K147 (F1L)	K137 (F1L)	K160 (F1L)	K98 (F1)	K295 (F2)
K138 (F1L)	K295 (F2)	K137 (F1L)	K149 (F1L)	K300 (F2)	K343 (F3)
K138 (F1L)	K196 (F1)	K149 (F1L)	K160 (F1L)	K98 (F1)	K300 (F2)
K138 (F1L)	K334 (F3)			K98 (F1)	K278 (F2)
				K106 (F1)	K300 (F2)
				K98 (F1)	K357 (F3)
				K66 (F0)	K268 (F2)

Table S5 SAXS data acquisition, sample details, data analysis, modeling, and software used.

(a) Sample details			
	t1-405	t1-405 (del30)	t1-405 (del37/GAG)
Organism	human	human	human
Source / expression system	<i>E. coli</i>	<i>E. coli</i>	<i>E. coli</i>
Description			
UniProt Q9Y490 residues 1-405 with N-terminal His-tag with linker (38 residues)	wild-type	residues 139-168 deleted	residues 134-170 replaced by Gly-Ala-Gly
Extinction coefficient (with all Cys residues reduced)	0.973	1.045	1.061
Partial specific volume ($\text{cm}^3 \text{ g}^{-1}$)	0.736	0.736	0.736
Particle contrast from sequence and solvent constituents (10^{10} cm^{-2})	2.85 (12.33-9.49)	2.84 (12.33-9.49)	2.83 (12.32-9.49)
M from chemical composition (Da)	51276	47702	46997
SEC-SAXS column	Superdex 200 10/300 GL		
Loading concentration (mg ml^{-1})	10.3	13.6	8.17
Injection volume (μl)	100		
Flow rate (ml min^{-1})	0.25		
Average concentration in combined data frames (mg ml^{-1})	0.71 (0.68-0.73)	0.68 (0.65-0.68)	0.60 (0.54-0.64)
Solvent (solvent blanks taken from SEC flow-through prior to and after elution of protein)	50 mM sodium phosphate, 150 mM NaCl, pH 7.2		
(b) SAXS data collection parameters			
Source, instrument and reference	DESY, Hamburg, EMBL-P12 beamline at the PETRA III storage ring; equipped with Pilatus 2M detector (Blanchet et al., 2015)		
Wavelength	1.2399 Å		
Beam geometry	Beam size $0.2 \times 0.12 \text{ mm}^2$, sample-detector distance 3 m		
q -measurement range (\AA^{-1} or nm^{-1})	0.025201-4.81238 nm^{-1}		
Normalization	To transmitted beam intensity		
Method for monitoring radiation damage	frame by frame comparison		
Exposure time, number of exposures	0.995-s data frame measurements of SEC elusion, 2400 exposures/sample		
Sample temperature	+10 °C		
(c) Software employed for SAXS data reduction, analysis and interpretation			
SAXS data reduction	radial averaging with Radaver at the P12 beamline, solvent subtraction with Datop		

Calculation of extinction coefficient from sequence	ProtParam (Gasteiger et al., 2005) via https://web.expasy.org/protparam/
Calculation of partial specific volume and particle contrast from chemical composition	MULCh (Whitten et al., 2008) via http://smb-research.smb.usyd.edu.au/NCVWeb/input.jsp
Basic analyses	ATSAS 2.8.2 (Franke et al., 2017): Guinier calculated with Primusqt (Konarev et al., 2003) $p(r)$ calculated with Datgnom (Petoukhov et al., 2007) Porod volume calculated with Datporod
Ensemble modeling	Crysol (Svergun et al., 1995): calculation of scattering from crystal structure of individual subdomains Eom (Tria et al., 2015) via ATSAS online (https://www.embl-hamburg.de/biosaxs/atsas-online/)
3D graphic model representations	Eom models visualized with PyMOL 1.8.4.2 (Schrodinger)

(d) Structural parameters

Guinier Analysis	t1-405	t1-405 (del30)	t1-405 (del37/GAG)
$I(0)$ (arbitrary units)	3677.77 ± 14.84	3837.71 ± 14.62	3252.78 ± 16.36
R_g	3.35 ± 0.03	3.28 ± 0.03	2.97 ± 0.11
sR_g range	0.518-1.298	0.464-1.297	0.48-1.21
Fidelity (Primusqt)	0.75	0.80	0.66
M (Da) from $I(0)$ (ratio to expected value) (calculated using the Protocol 8A in Jeffries et al. 2016)	55729 (1.09)	63235 (1.33)	59399 (1.26)

$p(r)$ analysis	t1-405	t1-405 (del30)	t1-405 (del37/GAG)
$I(0)$ (arbitrary units)	3823 ± 7.89	3916 ± 9.09	3306 ± 10.6
R_g	3.48 ± 0.01	3.48 ± 0.01	3.10 ± 0.02
d_{\max}	11.49	9.65	10.18
s range	0.1587-4.7978	0.1455-4.4582	0.1627-2.6924
Total estimate (Datgnom)	0.921	0.871	0.9206
M from $I(0)$ (ratio to expected value)	56867 (1.11)	62033 (1.30)	59451 (1.26)
V_P (Datporod)	90.90	76.33	70.42

(e) Atomistic modeling

Eom	t1-405	t1-405(del30)	t1-405(del37/GAG)
Crystal structures	PDB entry 3IVF (Elliott et al., 2010) residues 2-83, 87-133, 173-196, 202-304, 309-398 (F1 subdomain residues 87-133 and 173-196 constrained)		
Flexible regions (all: 84-86, 197-201, 305-308, 399-405)	134-172	134-139 + 169-172	GAG + 171-172
s range for fitting	0.1547-4.8124	0.1415-4.8124	0.1627-4.8124

Symmetry assumptions	P1	P1	P1
Flexibility (Rflex / R σ)	73.29% (84.93%) / 0.62	71.07% (87.05%) / 0.51	67.06% (87.04%) / 0.43
χ^2 , CorMap (Franke et al., 2015) p-values	1.661, 0.823	1.642, 0.824	2.046, 0.348
Constant subtracted	2.784	2.878	-1.821
Number of representative structures	4	3	3

Table S6. FERM domains used for alignment with the FERM domain of talin1

Protein	PDB ID	Reference
Human unconventional myosin 7A (1st FERM)	3PVL	Wu et al., 2011
Human unconventional myosin 7A (2nd FERM)	5MV9	Yu et al., 2017
Human unconventional myosin 7B (2nd FERM)	5XBF	Li et al., 2017a
Human unconventional myosin 10	3AU5	Hirano et al., 2011
SNX17	4GXB	Ghai et al., 2013
KRIT1	4HDO	Gingras et al., 2013
protein 4.1R	3QIJ	Nedyalkova et al., 2011
EPB41L3	2HE7	Busam et al., 2011
merlin	1H4R	Kang et al., 2002
ezrin	1NI2	Smith et al., 2003
moesin	1EF1	Pearson et al., 2000
TYK2	4PO6	Wallweber et al., 2014
JAK1	5IXD	Ferrao et al., 2016
JAK2	4Z32	McNally et al., 2016
mouse kindlin-2	5XPY	Li et al., 2017b
myosin VIIb (1st FERM domain)	5F3Y	Li et al., 2016
radixin	1J19	Hamada et al., 2000
chicken FAK1	2AL6	Ceccarelli et al., 2006

References

- Blanchet, C.E., A. Spilotros, F. Schwemmer, M.A. Graewert, A. Kikhney, C.M. Jeffries, D. Franke, D. Mark, R. Zengerle, F. Cipriani, S. Fiedler, M. Roessle, and D.I. Svergun. 2015. Versatile sample environments and automation for biological solution X-ray scattering experiments at the P12 beamline (PETRA III, DESY). *J. Appl. Crystallogr.* 48:431–443.
doi:10.1107/S160057671500254X.
- Capra, J.A., and M. Singh. 2007. Predicting functionally important residues from sequence conservation. *Bioinformatics*. 23:1875–1882. doi:10.1093/bioinformatics/btm270.
- Dephoure, N., C. Zhou, J. Villén, S.A. Beausoleil, C.E. Bakalarski, S.J. Elledge, and S.P. Gygi. 2008. A quantitative atlas of mitotic phosphorylation. *Proc. Natl. Acad. Sci.* 105:10762–10767. doi:10.1073/pnas.0805139105.
- Eaton, J.W., D. Bateman, S. Hauberg, and R. Wehbring. 2015. GNU Octave version 4.0.0 manual: a high-level interactive language for numerical computations.
- Edgar, R.C. 2004. MUSCLE: multiple sequence alignment with high accuracy and high throughput. *Nucleic Acids Res.* 32:1792–1797. doi:10.1093/nar/gkh340.

- Elliott, P.R., B.T. Goult, P.M. Kopp, N. Bate, J.G. Grossmann, G.C.K. Roberts, D.R. Critchley, and I.L. Barsukov. 2010. The Structure of the Talin Head Reveals a Novel Extended Conformation of the FERM Domain. *Structure*. 18:1289–1299. doi:10.1016/j.str.2010.07.011.
- Franke, D., C.M. Jeffries, and D.I. Svergun. 2015. Correlation Map, a goodness-of-fit test for one-dimensional X-ray scattering spectra. *Nat. Methods*. 12:419–422. doi:10.1038/nmeth.3358.
- Franke, D., M. V. Petoukhov, P. V. Konarev, A. Panjkovich, A. Tuukkanen, H.D.T. Mertens, A.G. Kikhney, N.R. Hajizadeh, J.M. Franklin, C.M. Jeffries, and D.I. Svergun. 2017. ATSAS 2.8 : a comprehensive data analysis suite for small-angle scattering from macromolecular solutions. *J. Appl. Crystallogr.* 50:1212–1225. doi:10.1107/S1600576717007786.
- Gasteiger, E., C. Hoogland, A. Gattiker, S. Duvaud, M.R. Wilkins, R.D. Appel, and A. Bairoch. 2005. Protein Identification and Analysis Tools on the ExPASy Server. In The Proteomics Protocols Handbook. J.M. Walker, editor. Humana Press. 571–607.
- Konarev, P. V, V. V Volkov, A. V Sokolova, M.H.J. Koch, and D.I. Svergun. 2003. PRIMUS: a Windows PC-based system for small-angle scattering data analysis. *J. Appl. Crystallogr.* 36:1277–1282. doi:10.1107/S0021889803012779.
- Kumar, S., G. Stecher, and K. Tamura. 2016. MEGA7: Molecular Evolutionary Genetics Analysis Version 7.0 for Bigger Datasets. *Mol. Biol. Evol.* 33:1870–1874. doi:10.1093/molbev/msw054.
- Petoukhov, M. V, P. V Konarev, A.G. Kikhney, and D.I. Svergun. 2007. ATSAS 2.1 -- towards automated and web-supported small-angle scattering data analysis. *J. Appl. Crystallogr.* 40:s223–s228. doi:10.1107/S0021889807002853.
- Pinon, P., J. Pärssinen, P. Vazquez, M. Bachmann, R. Rahikainen, M.-C. Jacquier, L. Azizi, J.A. Määttä, M. Bastmeyer, V.P. Hytönen, and B. Wehrle-Haller. 2014. Talin-bound NPLY motif recruits integrin-signaling adapters to regulate cell spreading and mechanosensing. *J. Cell Biol.* 205:265–281. doi:10.1083/jcb.201308136.
- Ratnikov, B., C. Ptak, J. Han, J. Shabanowitz, D.F. Hunt, and M.H. Ginsberg. 2005. Talin phosphorylation sites mapped by mass spectrometry. *J. Cell Sci.* 118:4921–4923. doi:10.1242/jcs.02682.
- Stuart, S.A., S. Houel, T. Lee, N. Wang, W.M. Old, and N.G. Ahn. 2015. A Phosphoproteomic Comparison of B-RAFV600E and MKK1/2 Inhibitors in Melanoma Cells. *Mol. Cell. Proteomics*. 14:1599–1615. doi:10.1074/mcp.M114.047233.
- Svergun, D., C. Barberato, and M.H.J. Koch. 1995. CRY SOL – a Program to Evaluate X-ray Solution Scattering of Biological Macromolecules from Atomic Coordinates. *J. Appl. Cryst.* 28:768–773.
- Tria, G., H.D.T. Mertens, M. Kachala, and D.I. Svergun. 2015. Advanced ensemble modelling of flexible macromolecules using X-ray solution scattering. *IUCrJ*. 2:207–217. doi:10.1107/S205225251500202X.
- Whitten, A.E., S. Cai, and J. Trehewella. 2008. MULCh : modules for the analysis of small-angle neutron contrast variation data from biomolecular assemblies. *J. Appl. Crystallogr.* 41:222–226. doi:10.1107/S0021889807055136.
- Zhu, L., J. Yang, T. Bromberger, A. Holly, F. Lu, H. Liu, K. Sun, S. Klapproth, J. Hirbawi, T. V. Byzova, E.F. Plow, M. Moser, and J. Qin. 2017. Structure of Rap1b bound to talin reveals a pathway for triggering integrin activation. *Nat. Commun.* 8:1744. doi:10.1038/s41467-017-01822-8.